Paleoceanography and Paleoclimatology

RESEARCH ARTICLE
10.1029/2018PA003481

Two-Timescale Carbon Cycle Response to an AMOC Collapse

Søren B. Nielsen[1], Markus Jochum[1], Joel B. Pedro[2,3], Carsten Eden[4], and Roman Nuterman[1]

[1]Climate and Computational Geophysics, Niels Bohr Institute, University of Copenhagen, Copenhagen, Denmark, [2]Antarctic Climate and Ecosystems CRC, University of Tasmania, Hobart, Tasmania, Australia, [3]UNI Research AS, Bergen, Norway, [4]Institut für Meereskunde, University of Hamburg, Hamburg, Germany

Key Points:
- Using an Earth System Model, we find a two-timescale response in the carbon cycle due to a reduction in Atlantic overturning
- A rapid increase in atmospheric carbon dioxide is related to tropical outgassing due to a shift in the tropical precipitation pattern
- A slow outgassing from the ocean is caused by a combination of reduced biological activity and increased ventilation rates

Correspondence to:
S. B. Nielsen,
soeren.nielsen@nbi.ku.dk

Citation:
Nielsen, S. B., Jochum, M., Pedro, J. B., Eden, C., & Nuterman, R. (2019). Two-timescale carbon cycle response to an AMOC collapse. *Paleoceanography and Paleoclimatology*, *34*. https://doi.org/10.1029/2018PA003481

Received 28 SEP 2018
Accepted 12 MAR 2019
Accepted article online 18 MAR 2019

Abstract Atmospheric CO_2 concentrations (pCO_2) varied on millennial timescales in phase with Antarctic temperature during the last glacial period. A prevailing view has been that carbon release and uptake by the Southern Ocean dominated this millennial-scale variability in pCO_2. Here, using Earth System Model experiments with an improved parameterization of ocean vertical mixing, we find a major role for terrestrial and oceanic carbon releases in driving the pCO_2 trend. In our simulations, a change in Northern Hemisphere insolation weakens the Atlantic Meridional Overturning Circulation (AMOC) leading to increasing pCO_2 and Antarctic temperatures. The simulated rise in pCO_2 is caused in equal parts by increased CO_2 outgassing from the global ocean due to a reduced biological activity and changed ventilation rates, and terrestrial carbon release as a response to southward migration of the Intertropical Convergence Zone. The simulated terrestrial release of carbon could explain stadial declines in organic carbon reservoirs observed in recent ice core $\delta^{13}C$ measurements. Our results show that parallel variations in Antarctic temperature and pCO_2 do not necessitate that the Southern Ocean dominates carbon exchange; instead, changes in carbon flux from the global ocean and land carbon reservoirs can explain the observed pCO_2 (and $\delta^{13}C$) changes.

1. Introduction

During the last glacial Greenland temperatures experienced abrupt fluctuations between warm (interstadial) and cold (stadial) conditions as observed in ice core water stable isotopes, often referred to as Dansgaard-Oeschger (DO) events (Dansgaard et al., 1993). DO events appear to be part of a major, global reorganization of the climate system. Associated with the Greenland interstadials is an increase in monsoon strength in China (Wang et al., 2001) and a decrease in monsoon strength in the southern South America (Kanner et al., 2012; Wang et al., 2006). Stadials are characterized by an opposite hemispheric monsoon response, as well as reduced strength of the Atlantic Meridional Overturing Circulation (AMOC) inferred from Pa/Th ratios (Böhm et al., 2015; Henry et al., 2016). Antarctica tends to warm during the Greenland stadials and cool during the Greenland interstadials (EPICA community members, 2006; WAIS Divide Project Members, 2015). The peaks in Antarctic warming, termed Antarctic Isotope Maximum (AIM) events, are the largest of these and are accompanied by increases in atmospheric CO_2 conentrations (pCO_2) by up to 20 ppmv (Ahn & Brook, 2008, 2014).

Recent measurements of $\delta^{13}C$ of air trapped in ice core bubbles show that $\delta^{13}C$ decreased in phase with rising pCO_2 during the Marine Isotope Stage 3 (MIS3) stadials, which suggests an organic source of carbon to the atmosphere (Bauska et al., 2018). Organic sources of carbon could either be terrestrial release or changes in the marine biological activity.

The close relationship between Antarctic temperatures, pCO_2, and $\delta^{13}C$ changes in Atlantic intermediate waters during longer stadials lead Ahn and Brook (2008) to suggest a Southern Ocean control on the pCO_2 increase. Marine sediment core records of biogenic silica, a proxy for upwelling, also suggest an increase in Southern Ocean ventilation during stadials (Anderson et al., 2009), which could increase Southern Ocean outgassing of CO_2. Recent model studies support increased formation rate of Antarctic Bottom Water as a mechanism for increasing pCO_2 (Menviel et al., 2015, 2018).

Due to the evidence of weak Atlantic overturning during AIM events, numerical studies have analyzed the response of the carbon cycle to overturning collapses induced by freshwater forcing in the North Atlantic.

Studies of vegetation responses to AMOC collapses find loss of terrestrial carbon to the atmosphere in boreal regions (Scholze et al., 2003) or the tropics (Bozbiyik et al., 2011; Köhler et al., 2005; Obata, 2007). Other studies find increased atmospheric pCO_2 as a result of changed ocean dynamics from reduced strength of the biological pump (Schmittner, 2005; Schmittner & Galbraith, 2008).

The majority of previous studies have employed simplified model setups, either by decoupling the carbon cycle from the climate models (Köhler et al., 2005; Scholze et al., 2003) or by using models of intermediate complexity (Bouttes et al., 2012; Menviel et al., 2008, 2015). One common feature, regardless of the choice of model used, is that vertical mixing in the ocean is parameterized using a constant background diffusivity. Such parameterization does not take into account changes in the energy provided for mixing caused by breaking of internal waves, or changes in the local stratification caused by perturbations in the ocean forcing. However, drastic circulation changes induced by an AMOC collapse have been identified to cause intermediate warming of the ocean (e.g., Brown & Galbraith, 2016; Pedro et al., 2018). As a result, ocean stratification and mixing rates should be affected, leading to changes in heat and carbon storage as well as feedback on the circulation.

In this paper we present a fully coupled climate model with active biogeochemistry where a combination of mixing and insolation changes drives an AMOC shutdown, releasing CO_2 to atmosphere comparable to those associated with stadials. Our simulations consist of a 1,000-year spin-up and a 1,000-year-long perturbation simulation using an Earth System Model. The length of the simulations reveals a two-timescale response to the collapse of the overturning circulation, a fast response causing terrestrial release of carbon, and a slow oceanic release of carbon due to a reduced biological pump. A thousand years after the perturbation, the terrestrial and oceanic release of carbon each account for roughly half the pCO_2 difference to the control simulation.

Our setup is different from previous studies in two important ways. First of all, the collapse of the overturning circulation in our model is forced without freshwater forcing, but is instead a result of a combination of the climate state prior to insolation perturbation and the sea ice export to the North Atlantic following the perturbation. Thus, we do not force the model with any virtual salt fluxes but have the collapse of the overturning evolve internally, in line with recent studies suggesting that DO events can be triggered by stochastic forcing without freshwater forcing (Brown & Galbraith, 2016; Kleppin et al., 2015; Peltier & Vettoretti, 2014; Zhang et al., 2017). Second, we use a recent parameterization for vertical mixing, with which we can investigate feedbacks in the ocean system caused by large changes in the stratification (Nielsen et al., 2018; Olbers & Eden, 2013).

The paper is structured as follows. In section 2 the vertical mixing parameterization is briefly presented along with model and the experimental setup. Section 3 present the simulated response to the change in orbital forcing in terms of ocean circulation and carbon fluxes. The results are discussed in section 4 and finally a summary and conclusion is given in section 5.

2. Methods

2.1. Vertical Mixing

Breaking internal waves in the ocean convert small-scale turbulent kinetic energy to potential energy. This process has in ocean models historically been represented as a constant diffusivity (e.g., Bryan, 1987). Empirical parameterizations of tidal mixing have been added to the global background diffusivities (Jayne, 2009; St. Laurent et al., 2002; Simmons et al., 2004), and recently more sophisticated parameterizations that account for how the energy that is put into the internal waves and eventually lost by dissipation have recently been developed (Melet et al., 2016; Polzin, 2009; Olbers & Eden, 2013).

The parameterization of internal wave breaking has consequences for the heat and carbon storage in the ocean (Bryan, 1987). We hypothesize that the changed stratification resulting from an AMOC collapse affects the deep mixing of the ocean which has impact on the global biogeochemistry. In order to test this we apply a recently proposed vertical mixing parameterization, IDEMIX (Olbers & Eden, 2013).

Internal wave energy, E, and dissipation rate, ϵ_{IW}, are computed directly for each grid cell in the ocean, and by using the Osborn (1980) model a vertical diffusivity can be obtained. The equation for E becomes

$$\frac{\partial E}{\partial t} - \frac{\partial}{\partial z}\left(c_0 \tau_v \frac{\partial c_0 E}{\partial z}\right) - \nabla_h \cdot v_0 \tau_h \nabla_h v_0 E = -\epsilon_{\mathrm{IW}} + \mathcal{S}, \tag{1}$$

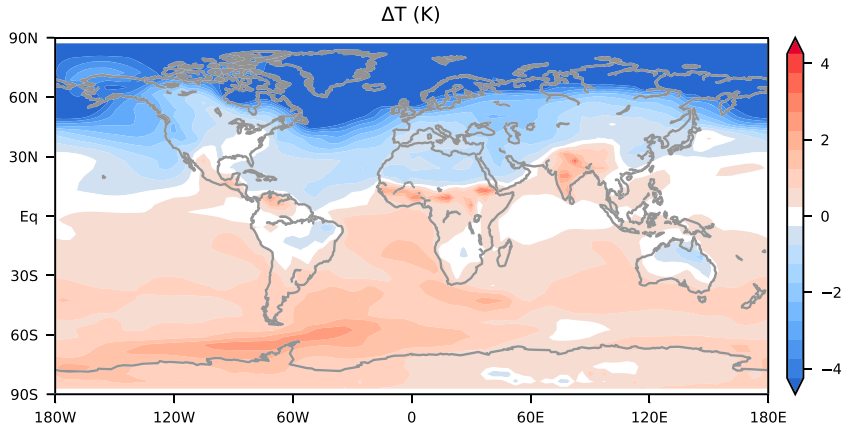

Figure 1. Surface temperature difference between THEN and CONT.

where c_0 and v_0 are the vertical and horizontal wave speeds, and τ_v and τ_h are vertical and horizontal elimination timescales of anisotropies in the wave field. S represents sources of energy. In our simulations we force IDEMIX with tides only (Jayne & St. Laurent, 2001). The diffusivity is calculated from the dissipation of internal wave energy and is parameterized as

$$\kappa = \frac{\delta}{1+\delta}\frac{\epsilon_{IW}}{N^2} = \frac{\delta}{1+\delta}\mu_0 f_e \frac{E^2}{c_\star^2 N^2} \tag{2}$$

where $c_\star = N^2/m_\star^2$ with $m_\star$ being the modal bandwidth, μ_0 a constant, and $f_e = f\text{arccosh}(N/f)$ and $\delta = 0.2$. For further description of the parameterization, we refer to previous studies (Eden & Olbers, 2014; Olbers & Eden, 2013; Pollmann et al., 2017).

2.2. Model Setup

We use the coarse resolution version of the Community Earth System Model version 1.2 (Danabasoglu et al., 2012; Gent et al., 2011; Hurrell et al., 2013; Shields et al., 2012). The ocean resolution varies with latitude so that zonal extent is 400 km near the Equator and 20 km at the poles, ranging from 400 to 40 km in the meridional resolution with largest values in the North Pacific. There are 60 vertical layers with nonuniform thickness, ranging from 10 m at the surface to 500 m at the bottom. The implementation of IDEMIX in CESM follows that of Nielsen et al. (2018). The ocean model is run with the Gent and McWilliams (1990) parameterization using a stratification-dependent thickness and isopycnal diffusivity (Danabasoglu & Marshall, 2007).

The atmospheric model uses a T31 spectral truncation in the horizontal with 26 vertical layers. Biogeochemistry is coupled to the climate system and actively exchanges carbon between ocean, atmosphere, and land. The ocean component includes diatoms, phytoplankton, and diazotrophs, with phytoplankton growth controlled by temperature, light, and available nutrients (N, P, Si, and Fe; Lindsay et al., 2014; Moore et al., 2004, 2013). The land component prognostically computes leaf and stem area indices and vegetation height using a prescribed spatial distribution of plant functional types (Lawrence et al., 2011; Lindsay et al., 2014).

The model is spun up from climatologies and an ocean at rest for 1,000 years using preindustrial (i.e., 1850 Common Era, CE) orbital forcing. At model year 1,000, the simulation branches in two, one control simulation using the same orbital configuration as in the spin-up, CONT, and one simulation where the orbital forcing is changed to that of 113,000 years before the Common Era (113 ka BCE). We will refer to this simulation as THEN. Both simulations are run for an additional 1,000 years. Analysis is carried out for the mean of the last 100 model years, unless stated otherwise.

Within the first two centuries after changing the orbital configuration, the AMOC strength measured at 26°N collapses from 12.5 Sv (Sverdrup, 1 Sv = 10^6 m^3/s) to below 5 Sv in THEN. The shutdown is a result of increased sea ice export from the Nordic Seas to the North Atlantic, increasing the surface stratification and inhibiting deep water formation (Jochum et al., 2010). By reducing the AMOC strength in this way we

Table 1
Overview of Model Runs Listing the Year of Orbital Configuration and pCO_2 and AMOC Strength Averaged Over the Last Hundred Years of Simulation

Case	Orbital configuration	pCO_2 (ppmv)	AMOC (Sv)
CONT	1850 CE	257.6	12.5
THEN	113 ka BCE	266.5	4.5

Note. AMOC = Atlantic Meridional Overturning Circulation; CE = Common Era; BCE = Before Common Era.

are free of any assumptions regarding localization and strength of an applied freshwater forcing, and the mechanism adds to the increasing number of processes that could have caused stadial conditions other than input of freshwater from ice sheets (e.g., Kleppin et al., 2015; Peltier & Vettoretti, 2014; Zhang et al., 2017). Whether the cause of Greenland stadials is related to direct input of freshwater or not, we note that Brown and Galbraith (2016) recently found that the global response of climate models to AMOC perturbation is robust to the choice of mechanism by which the AMOC is weakened.

We note that CONT has a reduction of pCO_2 of 30 ppmv compared to the preindustrial value that the model is initiated with, which is 287.4 ppmv. This can be attributed to the effects of the mixing parameterization, where in particular thermocline mixing is reduced compared to standard parameterizations using a fixed background diffusivity, causing the thermocline to be sharper and shallower, cooling the ocean, and increasing its solubility (Nielsen et al., 2018). As the ocean cools and solubility increases, this also reduces the radiative forcing of CO_2, acting as a positive feedback on ocean surface temperatures.

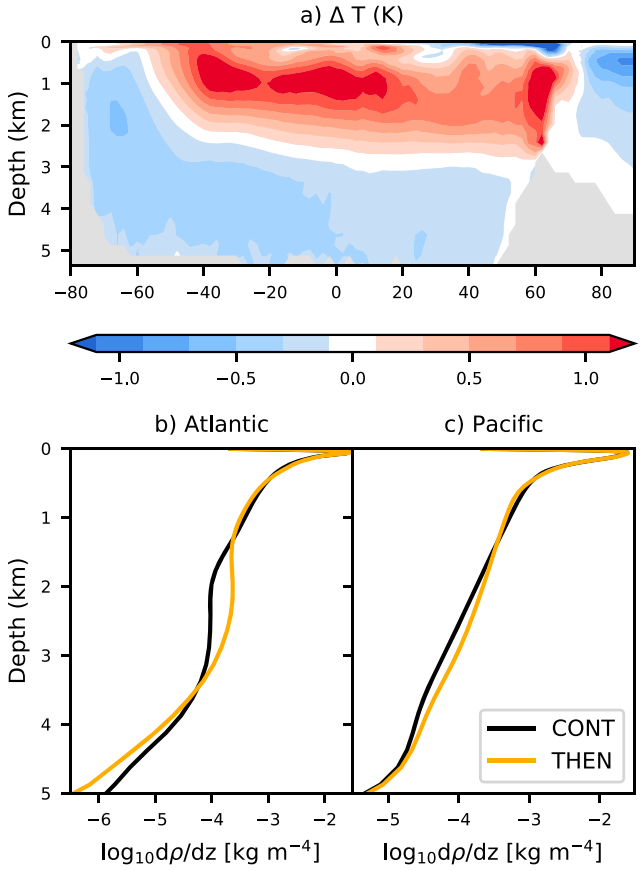

Figure 2. (a) Zonally averaged ocean temperature difference between THEN and CONT. (b) Ocean stratification averaged over the Atlantic basin for CONT (black) and THEN (yellow). (c) Same as (b) but for the Pacific Ocean.

3. Results

The surface temperature difference between the THEN and CONT, ΔT, is shown in Figure 1. The reduced oceanic heat transport from the Southern to the Northern Hemisphere results in a large-scale, bipolar temperature anomaly typical for simulations with collapsed overturning circulations (Brown & Galbraith, 2016; Pedro et al., 2018). The AMOC strength measured at 26°N is reduced from 12.5 Sv in CONT to just 4.5 Sv in THEN (see Table 1). As a result, strong cooling takes place in most of the Northern Hemisphere, in particular in the North Atlantic and Arctic where reduced heat transport results in expansion of the sea ice area in addition to the weaker summer insolation.

Figure 2a shows the zonally averaged ocean temperature difference between THEN and CONT. As discussed in Pedro et al. (2018), the AMOC collapse results in an intermediate warming of the ocean that spans the entire Atlantic Ocean until ~60°S where the Antarctic Circumpolar Current acts as a barrier for signal propagation (Cox, 1989; Huang et al., 2000; Schmittner et al., 2003). The deep ocean cools in THEN, which is caused by increased deep water formation in the Ross Sea (not shown). The intermediate warming and deep ocean cooling causes an increase in the Atlantic stratification between 1- and 3-km depth with a peak increase with more than a doubling at 2-km depth and a deep ocean decrease in stratification (Figure 2b), as well as a small increase in deep Pacific stratification below 2-km depth (Figure 2c).

The temperature evolution in the simulations shows a rapid decrease in temperature over Greenland of more than 6 K in THEN within the first few centuries of branching off, shown in Figure 3a. This temperature drop is at the lower end of estimated Greenland coolings during transitions into stadials (Kindler et al., 2014). For Antarctica (90–80°S), temperatures

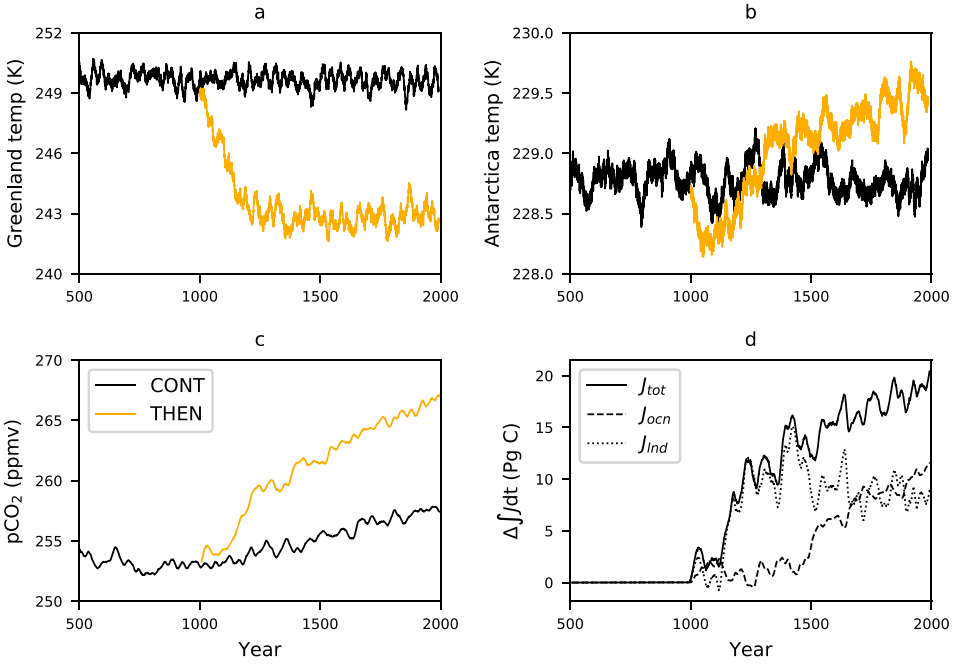

Figure 3. Time evolution (15-year running means, except for b) for CONT (black) and THEN (yellow). (a) Surface air temperature averaged over Greenland (70–80°N, 50–30°W). (b) Surface air temperature over Antarctica (80–90°S, 30-year running mean). (c) Globally averaged pCO_2. (d) Difference in cumulative flux of carbon to the atmosphere between THEN and CONT from the ocean (dashed), land (dotted), and total (solid).

initially drop, but rise a few centuries after the perturbation (Figure 3b). By the end of the simulation, Antarctica is ~0.5 K warmer in THEN than CONT. The rate of warming compares with that during AIM events, but the amplitude of warming falls short of the few Kelvin estimated for the largest AIMs. Here, however, the orbital configuration changes reduce solar insolation over Antarctica, as seen in the initial cooling in THEN, opposing the later warming caused by the AMOC collapse.

Compared to CONT, atmospheric pCO_2 in THEN increases rapidly within the first two centuries (Figure 3c) and then continues to rise slowly, but at a faster rate compared to CONT. By the end of the simulation, pCO_2 in THEN is ~9 ppmv larger than CONT (Table 1). This amounts to an almost 1 ppmv per century release of CO_2 to the atmosphere on average in THEN compared to CONT, which is comparable to observations from Antarctica over longer stadials (Ahn & Brook, 2014).

We separate the carbon fluxes, J_{tot}, into J_{ocn} (ocean-atmosphere fluxes) and J_{lnd} (land-atmosphere fluxes). The total change in pCO_2 is determined by the sum of the two,

$$\frac{\mathrm{d}pCO_2}{\mathrm{d}t} \propto J_{\mathrm{tot}} = J_{\mathrm{ocn}} + J_{\mathrm{lnd}}. \tag{3}$$

As fluxes vary strongly on interannual, annual, and seasonal timescales, we integrate equation (3) in time and compare the difference in cumulative fluxes between THEN and CONT, $\Delta \int J\mathrm{d}t$. The resulting curves are presented in Figure 3d. Solid lines denote total flux to the atmosphere, dashed lines ocean fluxes, and dotted lines terrestrial fluxes. Two timescales emerge to be relevant for the pCO_2 differences between the two simulations: a rapid terrestrial release of carbon between 100 and 300 years of perturbation in THEN, and a slow oceanic release of carbon. The initial increase in pCO_2 during the first century, roughly 1 ppmv, is caused by a terrestrial reorganization due to the insolation change. By the end of the simulation, each climate component has contributed by roughly half of the total increase in pCO_2. Where $\Delta \int J_{\mathrm{lnd}}\mathrm{d}t$ is slowly decreasing again after 500 years, that is, land reclaims carbon, $\Delta \int J_{\mathrm{ocn}}\mathrm{d}t$ continues to rise throughout the simulation.

We now investigate the fluxes related to each component of the carbon cycle, beginning with the fast terrestrial response.

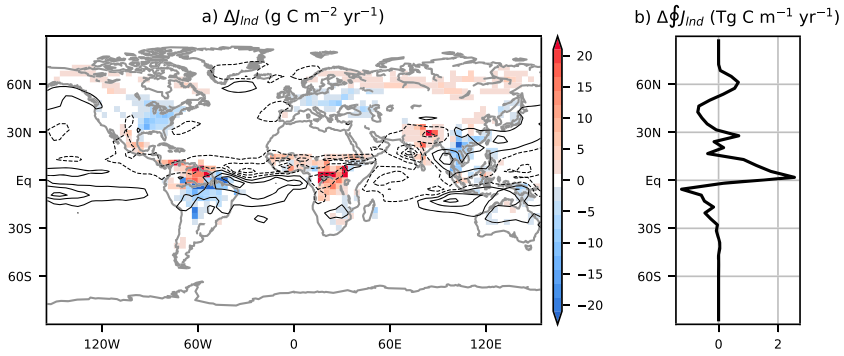

Figure 4. (a) Patterns of CO_2 flux differences from land to atmosphere between THEN and CONT averaged over model year 1100–1300 (positive anomalies denote carbon fluxes from land to atmosphere). Overlaid are contours of precipitation difference (contour interval is 0.5 mm/day, dashed lines denote negative precipitation difference). (b) Zonally integrated land-atmosphere CO_2 flux difference.

3.1. Land-Atmosphere Fluxes

The 8-Sv reduction in the AMOC strength causes a reduced Atlantic heat transport from the Southern to the Northern Hemisphere resulting in the ΔT patterns in Figure 1. This, in combination with the insolation change, shifts the latitude band of the tropical SST maximum which is linked to the position of the Intertropical Convergence Zone (ITCZ; e.g., Broccoli et al., 2006). Precipitation directly impacts the soil moisture, and precipitation anomalies can therefore lead to changes in the terrestrial carbon stock. As the major release of terrestrial carbon in THEN takes place between 100 and 300 years after the insolation change, we look at the ΔJ_{lnd} and precipitation anomalies averaged over this time interval. The difference in fluxes is shown in colors in Figure 4a. The black contours on top are precipitation anomalies. These show a decrease in tropical precipitation in the northern part of Amazon, India, and tropical Africa. These regions correspond to the areas of strongest release of terrestrial carbon. The regions of largest terrestrial carbon uptake,

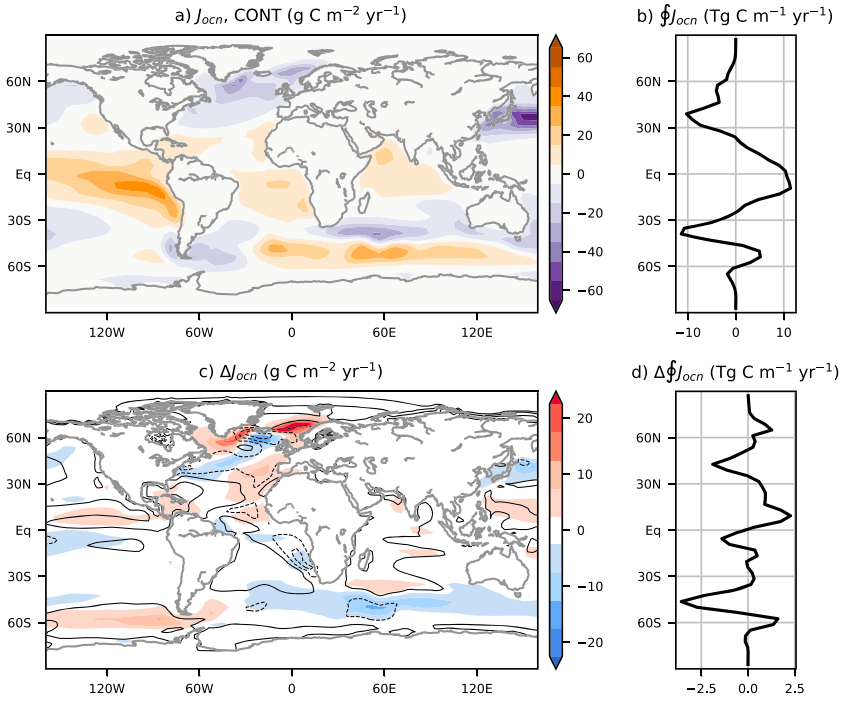

Figure 5. (a) Ocean-atmosphere fluxes of CO_2 (positive is outgassing) in CONT. (b) Zonally integrated ocean-atmosphere CO_2 flux for CONT. (c) Difference in surface fluxes between THEN and CONT. Overlaid are contours of the DIC difference averaged over the upper 150 m, with contour interval of 20 mmol/m^3 (solid contours denote increases in DIC). (d) Zonally integrated ocean-atmosphere CO_2 flux difference. DIC = dissolved inorganic carbon.

Table 2
Ocean to Atmosphere Fluxes in Runs Averaged Over the Last Hundred Years of Integration and Estimated Fluxes From Gruber et al. (2009)

Case	90–44°S	44–18°S	18°S to 18°N	18–49°N	49°N to 90°N	Total
CONT	0.142	−0.437	1.053	−0.496	−0.224	0.038
THEN	0.089	−0.472	1.107	−0.495	−0.180	0.049
Gruber et al. (2009)	0.4	−0.7	0.9	−0.5	−0.1	0.0

All units in petagrams carbon per year.

southern Amazon and Southeast Asia, are associated with increases in precipitation. When the flux differences are integrated zonally (Figure 4b), a strong tropical release emerges. This is dominated by the drought over tropical Africa and northern South America. The carbon release of the latter, as well as of India, is partly compensated by the increased uptake in the southern Amazon and south east Asia.

3.2. Ocean-Atmosphere Fluxes

The spatial patterns and zonal integral of ocean-atmosphere fluxes in CONT at the end of simulation are shown in Figures 5a and 5b, respectively. Table 2 lists the zonally integrated fluxes in the two simulations as well as inverse estimates of the present-day natural fluxes of carbon (Gruber et al., 2009). Comparing the latter to the fluxes in CONT shows that there is an overall agreement between the two, but discrepancies occur in the extratropical Southern Hemisphere, characterized by less outgassing south of 44°S and less uptake between 44 and 18°S in CONT compared to estimates. We note that the net Southern Hemisphere outgassing and uptake compare well, and that the discrepancies are related to a known equatorward shift of the Southern Hemisphere westerlies in CONT, which affects the latitude of upwelling and outgassing (Shields et al., 2012). Tropical outgassing is slightly larger in CONT and uptake equally larger in the northern high latitudes. Globally, a small net outgassing takes place in CONT.

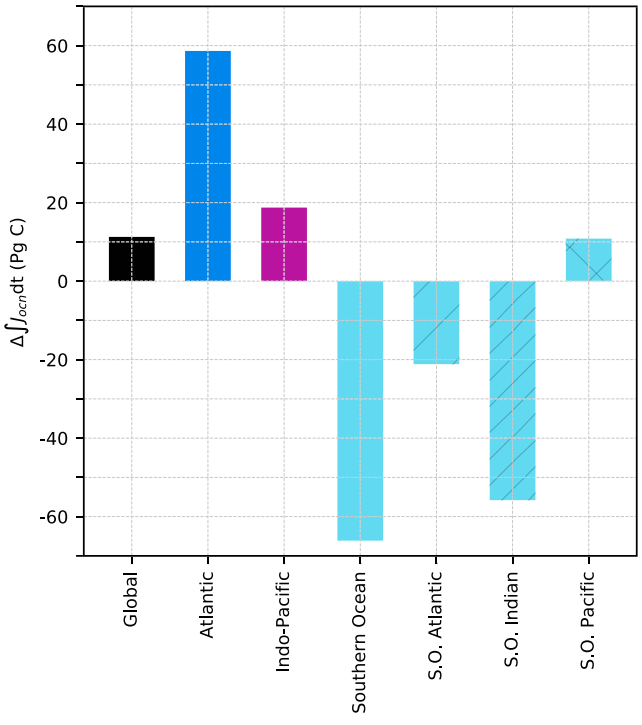

Figure 6. Difference in integrated fluxes from the ocean to the atmosphere (Pg C) separated into Global, Atlantic (including the Mediterranean and Northern Hemisphere high-latitude basins), Indo-Pacific, and Southern Ocean (defined as the ocean south of the latitude of the Cape of Good Hope). The Southern Ocean flux is the sum of the Atlantic (70°W to 25°E), Indian (25–140°E), and Pacific (140–290°E) sectors (hatched light blue bars on the right).

The large reorganization of the ocean circulation associated with the AMOC collapse leads to changes in carbon fluxes between THEN and CONT, ΔJ_{ocn}, shown in Figures 5c and 5d. When comparing fluxes between the two simulations we note that if not specified, outgassing (red in Figure 5c) may refer to either increased outgassing or reduced uptake in THEN, and uptake (blue in Figure 5c) refers to reduced outgassing or increased uptake. The differences between THEN and CONT can be summarized as follows: In the northern high latitudes, ocean uptake is reduced in THEN as a result of increased sea ice cover, inhibiting air-sea fluxes of carbon. In the northern midlatitudes, a near cancelation between flux anomalies occur between increased carbon uptake in the major current systems of the Kuroshiro and the Gulf Stream and increased outgassing in the midlatitude Atlantic. The Tropics are characterized by small changes, leading to an overall increase in outgassing, in particular, related to an overall small increase in Indian Ocean and west Pacific outgassing. The southern midlatitudes experience an increase in ocean uptake of carbon in the southern Pacific, partly compensated by a decreased uptake of carbon in the southern Indian Ocean. Finally, the net outgassing south of 44°S is reduced by more than one third.

As seen in previous studies (e.g., Jochum et al., 2010), the changes to air-sea fluxes of carbon is a patchwork of regional responses. In order to identify the important processes and regions we integrate the flux difference between THEN and CONT over different basins over time. We define the Southern Ocean as the ocean south of the latitude of the Cape of Good Hope, and the Atlantic includes the Mediterranean and high-latitude basins. Due to compensating flux differences we integrate

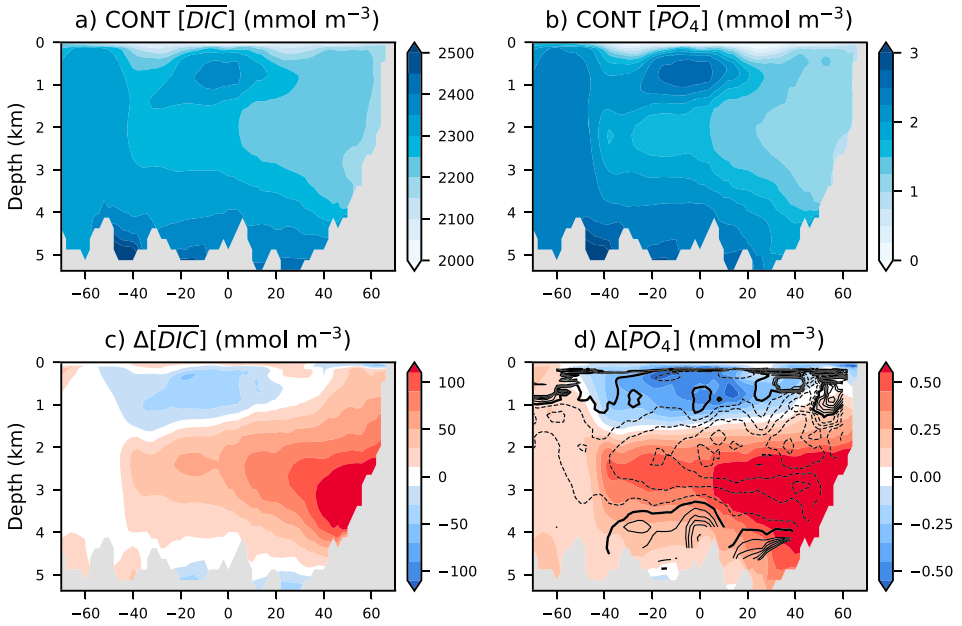

Figure 7. (a) Average DIC concentration in the Atlantic and Southern Ocean Atlantic sector in CONT (mmol/m^3). (b) Same as (a) but for PO_4 concentrations (mmol/m^3). (c) Difference in DIC concentrations between THEN and CONT (mmol/m^3). (d) Difference in PO_4 concentrations between THEN and CONT (mmol/m^3). Overlaid are meridionally smoothed contours of relative diffusivity in percent, contour interval 15%. Dashed contours indicate decreased diffusivities in THEN compared to CONT, highlighted contour is the 100% contour. DIC = dissolved inorganic carbon.

the Indo-Pacific as one basin. The resulting net fluxes of carbon at the end of the simulations are shown in Figure 6. The global integral yields a net flux of carbon from the ocean to the atmosphere in THEN of 11.3 Pg C compared to CONT. This flux is a sum of reduced uptake in the Atlantic and Indo-Pacific, largely compensated by a reduced outgassing in the Southern Ocean. As the Southern Ocean generally acts to lower atmospheric CO_2, contrary to existing hypotheses (Anderson & Carr, 2010), we will first investigate the reduced Southern Ocean outgassing, followed by the Atlantic and Indo-Pacific ougassing.

As Figure 5c shows that the separate regions of the Southern Ocean react differently to the changed forcing, we separate the integrated flux in the Southern Ocean into the Atlantic (70°W to 25°E), Indian (25–140°E) and Pacific (140–290°E) sectors, respectively (Figure 6). It is evident that the reduced outgassing in THEN is dominated by the Atlantic and Indian sectors, where outgassing of carbon from upwelled waters is reduced greatly (as also seen in Figure 5c), whereas the Pacific sector outgasses carbon of similar magnitude as the net global response.

In order to explain the reduced outgassing in the Atlantic and Indian sector of the Southern Ocean we plot contours the difference in dissolved inorganic carbon (DIC) concentrations averaged over the euphotic layer (the upper 150 m) over ΔJ_{ocn} in Figure 5c. This shows that the upwelled waters in the Atlantic and particularly Indian sector are depleted in DIC in THEN. The origin of this DIC depletion can be further illuminated by looking at the vertical structure of DIC in the Atlantic shown in Figure 7a for CONT and the difference between THEN and CONT seen in Figure 7c. DIC accumulates in the northern deep Atlantic in THEN, while south Atlantic intermediate waters get depleted in DIC. The DIC-depleted waters are entrained in the upwelling waters of the Atlantic and Indian sector of the Southern Ocean, leading to reduced concentration of CO_2 in the upwelled waters. Simultaneously, pCO_2 is increasing in THEN, leading to a decreased air-sea difference and as a result reduced outgassing in the Atlantic and Indian sector of the Southern Ocean.

The loss of carbon in the upper ocean (Figure 7a) is a global feature. Using apparent oxygen utilization, $AOU = O_{2sat} - O_2$, where O_{2sat} is the saturated O_2 concentration calculated from temperature and salinity, the remineralized, soft-tissue component, C_{soft}, of the total DIC is commonly estimated through the following relation (see, e.g., Lauderdale et al., 2013; Ödalen et al., 2018):

$$C_{soft} = r_{C:O_2} AOU. \quad (4)$$

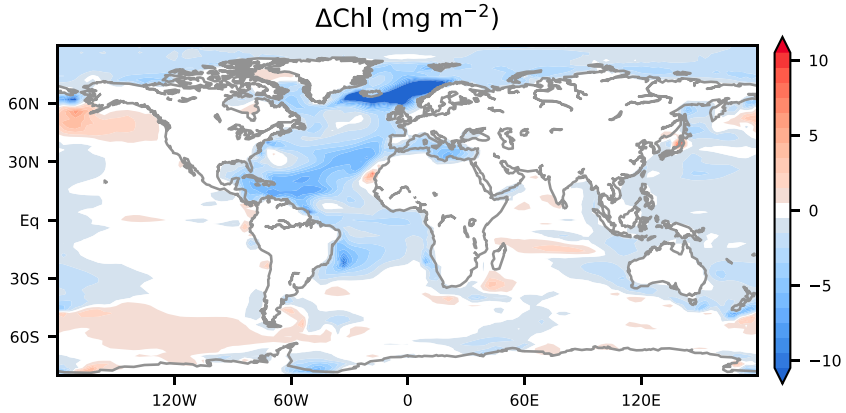

Figure 8. Difference in total chlorophyll content between THEN and CONT.

With a stoichiometric ratio $r_{C:O_2} = 117/170$ (Anderson & Sarmiento, 1994) one finds that the reduced upper and intermediate water column DIC is primarily lost as soft-tissue carbon, with a loss of almost 10% in the upper 1 km (not shown). The deep Atlantic DIC accumulation is also dominated by increased soft-tissue carbon from reduced ventilation. Due to disequilibrium effects, equation (4) overestimates C_{soft} in high latitude and deep waters (Ito et al., 2004). With a total outgassing difference of only 11.3 Pg between THEN and CONT, these uncertainties blur any marine carbon inventory analysis.

The East Pacific sector of the Southern Ocean, where an increase in oceanic outgassing to the atmosphere occurs, is characterized by the largest Southern Hemispheric warming (Figure 1) related to a reduced sea ice cover. The increased air-sea interaction from the reduced sea ice cover (as proposed by Stephens & Keeling, 2000) in combination with increased upwelling from a strengthening of the wind stress (see also Lee et al., 2011) leads to a stronger outgassing in this sector of the Southern Ocean. Thus, while the Southern Ocean as a whole acts as a sink for atmospheric CO_2, the increased ventilation in the Pacific sector cannot be neglected as a source for atmospheric carbon.

The increased outgassing from the Atlantic is a factor of 5 larger than the outgassing from the Pacific sector of the Southern Ocean. While the flux of carbon to the atmosphere is in part caused by the larger sea ice cover related to the shutdown of the overturning, inhibiting air-sea fluxes of carbon, the increase in North Atlantic stratification also reduces the depth of the winter mixed layer, which replenishes surface water nutrients. This leads to a decrease in the biological activity of the Atlantic (Schmittner, 2005). Figure 7b shows the average PO_4 concentration of the Atlantic and the Atlantic sector of the Southern Ocean (60°W to 16°E). Figure 7d shows the difference between THEN and CONT. The AMOC collapse leads to a depletion in nutrients in surface waters and an increase in deep ocean nutrients (Figure 7d). At the same time, the increased deep stratification in the Atlantic caused by intermediate warming (Figure 2b) causes a decrease in vertical diffusivity by more than 50% (Figure 7d, black contours). This reduces the rate at which nutrients are resupplied to the surface through internal wave breaking. As a result, nutrient supply is limited to coastal upwelling regions which are unaffected by the change in deep stratification. The reorganization of nutrients leads to a reduced biological activity in the Atlantic and leads to a reduction of the rate at which DIC is consumed in the surface waters. The result is a global reduction in primary production of roughly 10%, visualized in Figure 8 as a drop in chlorophyll content, in particular in the Atlantic, but also in the Pacific Ocean, in agreement with previous estimates of the marine ecosystem response to a collapse of the AMOC (Schmittner, 2005).

4. Discussion

Previous studies of the response of the carbon cycle to AMOC perturbations have generally found either a terrestrial source and oceanic sink of carbon (Bozbiyik et al., 2011; Menviel et al., 2008; Obata, 2007) or an oceanic source and terrestrial sink of carbon (Bouttes et al., 2012; Schmittner & Galbraith, 2008). A key result presented in the previous section is the two-timescale response of the Earth system to the

AMOC collapse resulting in contributions of increased pCO_2 by both climate components. Recent measurements from Taylor Glacier in Antarctica show that pCO_2 rose rapidly within a few centuries in phase with increased methane concentrations and a decrease in atmospheric $\delta^{13}C$ during MIS3 stadials, indicating an organic source of carbon (Bauska et al., 2018). This supports the idea of a tropical, terrestrial release of carbon related to a shift in precipitation associated with the ITCZ as seen in the present simulations. We note that the insolation forcing in the present setup not only triggers an AMOC collapse, but also in itself affects the tropical SST maximum, which could amplify or dampen the tropical precipitation response to the overturning weakening.

While the rapid carbon release can account for several ppmv of the increase during stadials, it is not enough to account for all stadial pCO_2 increase observed in ice cores (Ahn & Brook, 2014). The oceanic release takes centuries to start because outgassing is partly compensated by the rapid terrestrial release of carbon at the beginning of the perturbation. Once the terrestrial release ceases, oceanic outgassing continues and the terrestrial biosphere starts to act as a carbon sink. While the initial response resembles that of Bozbiyik et al. (2011) who used an older version of the same model, we note that their simulations only lasted 300 years, which we find is too short to identify the oceanic carbon flux response.

While the applied insolation forcing is abrupt, and a realistic, gradual transition could lead to a different model response, the climate and carbon cycle response of the present stimulations is still illuminating to explore as drastic perturbations to the insolation have occurred in the past (Pausata et al., 2015).

The present results find that after one millennium, in addition to the fast terrestrial release of carbon, the ocean accounts for an equal but more gradual release of CO_2 due to a combination of reduced biological activity, particularly in the Atlantic, and deep ocean ventilation in the Pacific sector of the Southern Ocean. While there is evidence of increased Southern Ocean upwelling during stadials (Anderson et al., 2009), recent ocean sediment $\delta^{11}B$ results from the Nordic Seas support the possible release of carbon in the North Atlantic (Ezat et al., 2017).

A reduced biological pump caused by an AMOC collapse in response to freshwater forcing in the North Atlantic was found by Schmittner and Galbraith (2008) to dominate the outgassing of CO_2 to the atmosphere during stadials, with a minor release from boreal vegetation. We also find large reductions in air-sea fluxes of carbon due to a reduced marine primary production. However, the present simulations differ in two important ways from the results of Schmittner and Galbraith (2008).

First, the major release of terrestrial carbon in our model occurs in the tropics rather than in the boreal regions, related to a shift in the ITCZ. The lack of a tropical response in the results of Schmittner and Galbraith (2008) is a direct result of the missing wind and precipitation changes in their energy-balance atmospheric model. Schmittner and Lund (2015) analyzed the sensitivity of the terrestrial carbon fluxes to a southward migration of the ITCZ and found a similar rapid release of terrestrial carbon to the atmosphere as seen in the present simulations. The missing boreal signal in the present results, on the other hand, may be related to the lack of dynamic vegetation in the land component. Scholze et al. (2003), using a dynamic vegetation model, found a large release of carbon in the Northern Hemisphere in response to an AMOC collapse, in part attributed to plant functional types being replaced by less productive types. Our simulations lack such mechanisms. As a consequence, the terrestrial release of carbon in response to an AMOC collapse could be even larger than shown here. However, Obata (2007) noted that the magnitude of terrestrial release of carbon depends strongly on the background climate prior to AMOC collapses. The terrestrial carbon inventory during the glacial was smaller than preindustrial values. As our simulations are carried out using a preindustrial configuration, the terrestrial carbon stock may be be smaller using glacial boundary conditions. Similarly, the ocean carbon inventory was likely larger during the last glacial (see, e.g., Sigman & Boyle, 2000), and thus the ocean outgassing in response to an AMOC weakening could be different in magnitude under such boundary conditions. However, we note that pCO_2 in CONT is lower than preindustrial, and conversely, the marine carbon inventory is larger. The weak AMOC in CONT, a bias in the coarse resolution CESM (Shields et al., 2012), also influences carbon sequestration through both solubility and particularly biology (Ödalen et al., 2018).

The second difference, with respect to Schmittner and Galbraith (2008), is that the biological activity of the Atlantic is reduced in our simulations not only because of the shallower winter mixed layer due to increased surface stratification but also due to the decreased mixing resulting from the increased ocean stratification.

While their model includes a tidal mixing parameterization, such dynamical feedback is damped in models with fixed background diffusivities and underlines the importance of improving understanding of forcing mechanisms of the internal wave field. In the present setup we use a fixed energy supply from the conversion of barotropic tides to internal waves and thus only find changes in mixing from changes in stratification. However, large changes occur in the surface wind stress due to the collapsing AMOC, which could alter the amount of energy entering the internal wave field from mesoscale eddy forcing or near-inertial waves. Furthermore, changing energy sources and stratification affects the overturning circulation (e.g., Schmittner et al., 2015). While the relative importance of the decreased diffusivities on the reduced biological activity in the present simulations is likely second order compared to the reduced deep winter mixing that replenishes surface waters with nutrients, it highlights the need for careful treatment of the vertical mixing in ocean models.

We note that changes in wind patterns also impact the ocean biogeochemistry through dust and iron supply. The present model uses a fixed climatology of dust and iron fluxes, and as a result has no changes in the iron supply due to the wind stress changes resulting from the AMOC collapse.

While the AMOC collapse results in increasing temperatures in the intermediate ocean (Figure 2a), an effect on pCO_2 from a reduced solubility pump can be present in our simulations. However, the global surface temperature difference is only 0.1 K. While this reduces the ocean solubility, it can account for only a small part of the observed pCO_2 increase (e.g., Omta et al., 2011).

Several studies suggest increased ventilation in the Southern Ocean as a mechanism for increased pCO_2 during stadials (Anderson et al., 2009; Menviel et al., 2015). This argument is partly based on increased opal burial, which indicates increased export production, also observed in the present simulations, most notably in the Pacific sector (Figure 8). Sediment and coral radiocarbon in the Southern Ocean also indicate increased ventilation during Heinrich stadial 1, coincident with an increase in atmospheric pCO_2 (Burke & Robinson, 2012; Skinner et al., 2010). The present simulations show increased Southern Ocean ventilation rates in agreement with these records (not shown). While the Pacific sector releases more carbon due to a decrease in sea ice cover, increased surface DIC and increased AABW formation in the Ross Sea, Southern Ocean outgassing is overall reduced due to the decrease in DIC concentrations of the upwelling waters in the Atlantic and Indian sector that entrain intermediate waters depleted in DIC.

The Pacific sector of the Southern Ocean, in agreement with previous studies, ventilates the Pacific, contributing to the net release of carbon (Menviel et al., 2014). However, we highlight that flux anomalies in the Southern Ocean are nonuniform and that local outgassing is influenced by remote processes. In the present simulation, reduced DIC concentrations in the upwelled waters in the Atlantic and Indian sector lead to decreased outgassing. To fully understand the role of the Southern Ocean on outgassing, further understanding of the spatial heterogeneity in carbon fluxes during the last glacial is needed.

As the outgassing from the Atlantic, Indo-Pacific, and Pacific sector of the Southern Ocean is largely compensated by reduced outgassing in the Atlantic and Indian sector of Southern Ocean, the present simulations find that a combination of tropical terrestrial release of carbon, reduced oceanic primary production, and increased ventilation in the Pacific sector of the Southern Ocean contribute to rising atmospheric pCO_2 in response to a strong weakening of the AMOC. Since the overturning likely weakened during stadials (Böhm et al., 2015; Henry et al., 2016), we speculate that these mechanisms could be important for the pCO_2 increase during stadials.

5. Summary and Conclusions

We simulate the response of the carbon cycle in an Earth System Model due to a collapse of the overturning over 1,000 years. The main results can be summarized as follows:

1. A simulated collapse of the AMOC leads to a two-timescale response in the carbon cycle, consisting of a rapid terrestrial release and a slow, oceanic outgassing of carbon.
2. The terrestrial release is attributed to changes in precipitation in the tropics related to shifts in the ITCZ over South America and Asia, as well as drought over Africa.
3. The ocean outgassing is attributed to a combination of a shallower winter mixed layer depth in the Atlantic and reduced diapycnal mixing, both of which limit the nutrient supply to the surface waters. This, in turn, reduces biological activity and associated carbon uptake globally.

4. The Southern Ocean outgassing is overall reduced as upwelling waters in the Atlantic and Indian sector of the Southern Ocean are depleted in DIC, leading to regionally reduced outgassing, whereas the Pacific sector outgasses more carbon to the atmosphere.

Acknowledgments
This study was supported by the Danish Council for Independent Research, Natural Sciences, 4002-00397. Simulations were done with support from the Danish Centre for Climate Computing at the University of Copenhagen. J. B. P. was supported by the European Research Council under the European Community's Seventh Framework Programme (FP7/2007e2013)/ERC grant agreement 610055 as part of the ice2ice project. Ocean and atmospheric model output means are available online at this website (https://sid.erda.dk/wsgi-bin/ls.py?share_id=h92uPoX96j). Other output fields are available from the lead author upon request.

References

Ahn, J., & Brook, E. J. (2008). Atmospheric CO_2 and climate on millennial time scales during the last glacial period. *Science*, *322*, 83–85.
Ahn, J., & Brook, E. J. (2014). Siple dome ice reveals two modes of millenial CO_2 change during the last ice age. *Nature Communications*, *5*, 3723.
Anderson, R. F., Ali, S., Bradtmiller, L. I, Nielsen, S. H. H., Fleischer, M. Q., Anderson, L. H., & Burckle, B. E. (2009). Wind-driven upwelling in the Southern Ocean and the deglacial rise in atmospheric CO_2. *Science*, *323*, 1443–1448.
Anderson, R. F., & Carr, M.-E. (2010). Uncorking the Southern Ocean's vintage CO_2. *Science*, *328*, 1117–1118.
Anderson, L. A., & Sarmiento, J. L. (1994). Redfield ratios of remineralization determined by nutrient data analysis. *Global Biogeochemical Cycles*, *8*, 65–80.
Bauska, T. K., Brook, E. J., Marcott, S. A., Baggenstos, D., Shackleton, S., Severinghaus, J. P., & Petrenko, V. V. (2018). Controls on millennial-scale atmospheric CO_2 variability during the last glacial period. *Geophysical Research Letters*, *45*, 7731–7740. https://doi.org/10.1029/2018GL077881
Böhm, E., Lippold, J., Gutjahr, M., Frank, M., Blaser, P., Antz, B., et al. (2015). Strong and deep Atlantic meridional overturning circulation during the last glacial cycle. *Nature*, *517*, 73–76.
Bouttes, N., Roche, D. M., & Paillard, D. (2012). Systematic study of the impact of fresh water fluxes on the glacial carbon cycle. *Climate of the Past*, *8*(2), 589–607.
Bozbiyik, A., Steinacher, M., Joos, F., Stocker, T. F., & Menviel, L. (2011). Fingerprints of changes in the terrestrial carbon cycle in response to large reorganizations in ocean circulation. *Climate of the Past*, *7*(1), 319–338.
Broccoli, A. J., Dahl, K. A., & Stouffer, R. J. (2006). Response of the ITCZ to Northern Hemisphere cooling. *Geophysical Research Letters*, *33*, L01702. https://doi.org/10.1029/2005GL024546
Brown, N., & Galbraith, E. D. (2016). Hosed vs. unhosed: Interruptions of the Atlantic Meridional Overturning Circulation in a global coupled model, with and without freshwater forcing. *Climate of the Past*, *12*, 1663–1679.
Bryan, F. (1987). Parameter sensitivity of primitive equation ocean general circulation models. *Journal of Physical Oceanography*, *17*, 970–985.
Burke, A., & Robinson, L. F. (2012). The Southern Ocean's role in carbon exchange during the last deglaciation. *Science*, *335*, 557–561.
Cox, M. D. (1989). An idealized model of the world ocean. Part 1: The global-scale water masses. *Journal of Physical Oceanography*, *19*, 1730.
Danabasoglu, G., Bates, S. C., Briegleb, B. P., Jayne, S. R., Jochum, M., Large, W. G., et al. (2012). The CCSM4 ocean component. *Journal Climate*, *25*, 1361–1389.
Danabasoglu, G., & Marshall, J. (2007). Effects of vertical variations of thickness diffusivity in an ocean general circulation model. *Ocean Modelling*, *18*, 122–141.
Dansgaard, W., Johnsen, S. J., Clause, H. B., Dahl-Jensen, D., Gundestrup, N. S., Hammer, C. U., et al. (1993). Evidence of general instability of past climate from a 250-kyr ice-core record. *Nature*, *364*, 218–220.
EPICA community members (2006). One-to-one coupling of glacial climate variability in Greenland and Antarctica. *Nature*, *444*, 196–198.
Eden, C., & Olbers, D. (2014). An energy compartment model for propagation, nonlinear interaction, and dissipation of internal gravity waves. *Journal of Physical Oceanography*, *44*, 2093–2106.
Ezat, M. M., Rasmussen, T. L., Hönisch, B., Groeneveld, J., & deMenocal, P. (2017). Episodic release of CO_2 from the high-latitude North Atlantic Ocean during the last 135 kyr. *Nature Communications*, *8*, 14498.
Gent, P. R., Danabasoglu, G., Donner, L. J., Holland, M. M., Hunke, E. C., Jayne, S. R., et al. (2011). The community climate system model version 4. *Journal Climate*, *24*, 4973–4991.
Gent, P. R., & McWilliams, J. C. (1990). Isopycnal mixing in ocean circulation models. *Journal of Physical Oceanography*, *20*, 150–155.
Gruber, N., Gloor, M., Mikaloff, F., Sara, E., Doney, S. C., Dutkiewicz, S., et al. (2009). Oceanic sources, sinks and transport of atmospheric CO_2. *Global Biogeochemical Cycles*, *23*, GB1005. https://doi.org/10.1029/2008GB003349
Henry, L. G., McManus, J. F., Curry, W. B., Roberts, N. L., Piotrowski, A. M., & Keigwin, L. D. (2016). North Atlantic Ocean circulation and abrupt climate change during the last glaciation. *Science*, *353*, 470–474.
Huang, R. X., Cane, M. A., Naik, N., & Goodman, P. (2000). Global adjustment of the thermocline in response to deepwater formation. *Geophysical Research Letters*, *27*, 759–762.
Hurrell, J. W., Holland, M. M., Gent, P. R., Ghan, S. J., Kay, J., Kushner, P., et al. (2013). The community earth system model—A framework for collaborative research. *Bulletin of the American Meteorological Society*, *94*, 1339–1360.
Ito, T., Follows, M. J., & Boyle, E. A. (2004). Is AOU a good measure of respiration in the oceans? *Geophysical Research Letters*, *31*, L17305. https://doi.org/10.1029/2004GL020900
Jayne, S. R. (2009). The impact of abyssal mixing parameterizations in an ocean general circulation model. *Journal of Physical Oceanography*, *39*, 1756–1775.
Jayne, S. R., & St. Laurent, L. C. (2001). Parameterizing tidal dissipation over rough topography. *Geophysical Research Letters*, *28*(5), 811–814.
Jochum, M., Peacock, S., Moore, K., & Lindsay, K. (2010). Response of air-sea carbon fluxes and climate to orbital forcing changes in the community climate system model. *Paloceanography*, *25*, PA3201. https://doi.org/10.1029/2009PA001856
Kanner, L. C., Burns, S. J., Cheng, H., & Edwards, R. L. (2012). High-latitude forcing of the South American summer monsoon during the last glacial. *Science*, *335*, 570–573.
Kindler, P., Guillevic, M., Baumgartner, M., Schwander, J., Landais, A., & Leuenberger, M. (2014). Temperature reconstruction from 10 to 120 kyr b2k from the NGRIP ice core. *Climate of the Past*, *10*, 887–902.
Kleppin, H., Jochum, M., Otto-Bliesner, B., Shields, C. A., & Yeager, S. (2015). Stochastic atmospheric forcing as a cause of Greenland climate transitions. *Journal Climate*, *28*, 7741–7763.
Köhler, P., Joos, F., Gerber, S., & Knutti, R. (2005). Simulated changes in vegetation distribution, land carbon storage, and atmospheric CO_2 in response to a collapse of the North Atlantic thermohaline circulation. *Climate Dynamics*, *25*(7), 689–708.
Lauderdale, J. M., Naveira Garabato, A. C., Oliver, K. I. C., Follows, M. J., & Williams, R. G. (2013). Wind-driven changes in Southern Ocean residual circulation, ocean carbon reservoirs and atmospheric CO_2. *Climate Dynamics*, *41*, 2145–2164.

Lawrence, D. M., Oleson, K. W., Flanner, M. G., Thornton, P. E., Swenson, S. C., Lawrence, P. J., et al. (2011). Parameterization improvements and functional and structural advances in version 4 of the community land model. *Journal of Advances in Modeling Earth Systems*, *3*, M03001. https://doi.org/10.1029/2011MS000045

Lee, S.-Y., Chiang, J. C. H., Matsumoto, K., & Tokos, K. S. (2011). Southern Ocean wind response to North Atlantic cooling and the rise in atmospheric CO_2: Modeling perspective and paleoceanographic implications. *Paleoceanography*, *26*, PA1214. https://doi.org/10.1029/2010PA002004

Lindsay, K., Bonan, G. B., Doney, S. C., Hoffman, F. M., Lawrence, D. M., Long, M. C., et al. (2014). Preindustrial-control and twentieth-century carbon cycle experiments with the Earth System Model CESM1(BGC). *Journal Climate*, *27*, 8981–9005.

Melet, A., Legg, S., & Hallberg, R. (2016). Climate impacts of parameterized local and remote tidal mixing. *Journal Climate*, *29*, 3473–3500.

Menviel, M. H., England, L., Meissner, K. J., Mouchet, A., & Yu, J. (2014). Atlantic-Pacific seesaw and its role in outgassing CO_2 during Heinrich events. *Paleoceanography*, *29*, 58–70. https://doi.org/10.1002/2013PA002542

Menviel, L., Spence, P., & England, M. H. (2015). Contribution of enhanced Antarctic Bottom Water formation to Antarctic warm events and millennial-scale atmospheric CO_2 increase. *Earth and Planetary Science Letters*, *413*, 37–50.

Menviel, L., Spence, P., Yu, J., Chamberlain, M. A., Matearm, R. J., Meissner, K. J., & England, M. H. (2018). Southern Hemisphere westerlies as a driver of the early deglacial atmospheric CO_2 rise. *Nature Communications*, *9*, 2503.

Menviel, L., Timmermann, A., Mouchet, A., & Timm, O. (2008). Meridional reorganization of marine and terrestrial productivity during Heinrich events. *Paleoceanography*, *23*, PA1203. https://doi.org/10.1029/2007PA001445

Moore, J. K., Doney, S. C., & Lindsay, K. (2004). Upper ocean ecosystem dynamics and iron cycling in a global three-dimensional model. *Global Biogeochemical Cycles*, *18*, GB4028. https://doi.org/10.1029/2004GB002220

Moore, J. K., Lindsay, K., Doney, S. C., Long, M. C., & Misumi, K. (2013). Marine ecosystem dynamics and biogeochemical cycling in the Community Earth System Model [CESM1(BGC)]: Comparison of the 1990s with the 2090s under the RCP4.5 and RCP8.5 scenarios. *Journal Climate*, *26*, 9291–9312.

Nielsen, S. B., Jochum, M., Eden, C., & Nuterman, R. (2018). An energetically consistent vertical mixing parameterization in CCSM4. *Ocean Modelling*, *127*, 46–54.

Obata, A. (2007). Climate-carbon cycle model response to freshwater discharge into the North Atlantic. *Journal of Climate*, *20*(24), 5962–5976.

Ödalen, M., Nycander, J., Oliver, K. I. C., Brodeau, L., & Ridgwell, A. (2018). The influence of the ocean circulation state on ocean carbon storage and CO_2 drawdown potential in an Earth system model. *Biogeosciences*, *15*, 1367–1393.

Olbers, D., & Eden, C. (2013). A global model for the diapycnal diffusivity induced by internal gravity waves. *Journal of Physical Oceanography*, *43*, 1759–1779.

Omta, A. W., Dutkiewicz, S., & Follows, M. (2011). Dependence of the ocean-atmosphere partitioning of carbon on temperature and alkalinity. *Global Biogeochemical Cycles*, *25*, GB1003. https://doi.org/10.1029/2010GB003839

Osborn, T. R. (1980). Estimates of the local rate of vertical diffusion from dissipation measurements. *Journal of Physical Oceanography*, *10*, 83–89.

Pausata, F. S. R., Chafik, L., Caballero, R., & Battisti, D. S. (2015). Impacts of high-latitude volcanic eruptions on ENSO and AMOC. *Proceedings of the National Academy of Sciences of the United States of America*, *112*, 13,784–13,788.

Pedro, J., Jochum, M., Buizert, C., He, F., Barker, S., & Rasmussen, S. O. (2018). Beyond the bipolar seesaw: Toward a process understanding of interhemispheric coupling. *Quaternary Science Reviews*, *192*, 27–46.

Peltier, W. R., & Vettoretti, G. (2014). Dansgaard-Oeschger oscillations predicted in a comprehensive model of glacial climate: A "kicked" salt oscillator in the Atlantic. *Geophysical Research Letters*, *41*, 7306–7313. https://doi.org/10.1002/2014GL061413

Pollmann, F., Eden, C., & Olbers, D. (2017). Evaluating the global internal wave model IDEMIX using fine structure methods. *Journal of Physical Oceanography*, *47*, 2267–2289.

Polzin, K. L. (2009). An abyssal recipe. *Ocean Modelling*, *30*, 298–309.

Schmittner, A. (2005). Decline of the marine ecosystem caused by a reduction in the Atlantic overturning circulation. *Nature*, *434*, 628–633.

Schmittner, A., & Galbraith, E. D. (2008). Glacial greenhouse-gas fluctuations controlled by ocean circulation changes. *Nature*, *456*, 373–376.

Schmittner, A., Green, J. A. M., & Wilmes, S.-B. (2015). Glacial ocean overturning intensified by tidal mixing in a global circulation model. *Geophysical Research Letters*, *42*, 4014–4022. https://doi.org/10.1002/2015GL063561

Schmittner, A., & Lund, D. C. (2015). Early deglacial Atlantic overturning decline and its role in atmospheric CO_2 rise inferred from carbon isotopes δ^{13} C. *Climate of the Past*, *11*, 135–152.

Schmittner, A., Saenko, O. A., & Weaver, A. J. (2003). Coupling of the hemispheres in observations and simulations of glacial climate change. *Quaternary Science Reviews*, *22*, 659–671.

Scholze, M., Knorr, W., & Heimann, M. (2003). Modelling terrestrial vegetation dynamics and carbon cycling for an abrupt climatic change event. *The Holocene*, *13*(3), 327–333.

Shields, C. A., Bailey, D. A., Danabasoglu, G., Jochum, M., Kiehl, J. T., Levis, S., & Park, S. (2012). The low-resolution CCSM4. *Journal Climate*, *25*, 3993–4014.

Sigman, D. M., & Boyle, E. A. (2000). Glacial/interglacial variations in atmospheric carbon dioxide. *Nature*, *407*, 859–869.

Simmons, H. L., Jayne, S. R., St. Laurent, L. C., & Weaver, A. J. (2004). Tidally driven mixing in a numerical model of the ocean general circulation. *Ocean Modelling*, *6*, 245–263.

Skinner, L. C., Fallon, S., Waelbrock, C., Michel, E., & Barker, S. (2010). Ventilation of the deep Southern Ocean and deglacial CO_2 rise. *Science*, *328*, 1147–1151.

St. Laurent, L. C., Simmons, H. L., & Jayne, S. R. (2002). Estimating tidally driven mixing in the deep ocean. *Geophysical Research Letters*, *29*(23), 2106. https://doi.org/10.1029/2002GL015633

Stephens, B. B., & Keeling, R. F. (2000). The influence of Antarctic sea ice on glacial-interglacial CO_2 variations. *Nature*, *404*, 171–174.

WAIS Divide Project Members (2015). Precise interpolar phasing of abrupt climate change during the last ice age. *Nature*, *520*, 661–665.

Wang, X., Auler, A. S., Edwards, R. L., Cheng, H., Ito, E., & Solheid, M. (2006). Interhemispheric anti-phasing of rainfall during the last glacial period. *Quaternary Science Reviews*, *25*, 3391–3403.

Wang, Y. J., Cheng, H., Edwards, R. L., An, A. S., Wu, J. Y., Shen, C.-C., & Dorale, J. A. (2001). A high-resolution absolute-dated late Pleistocene monsoon record from Hulu Cave, China. *Science*, *294*, 2345–2348.

Zhang, X., Knorr, G., Lohmann, G., & Barker, S. (2017). Abrupt North Atlantic circulation changes in response to gradual CO_2 forcing in a glacial climate state. *Nature Geoscience*, *10*, 518–524.